Physics – Uspekhi **66** (7) 722 – 733 (2023)

INSTRUMENTS AND METHODS OF INVESTIGATION PACS numbers: 05.70.Fh, 05.70.Ln, **68.70.+w**

Electromagnetic levitation method as a containerless experimental technique

L V Toropova, D V Alexandrov, A Kao, M Rettenmayr, P K Galenko

DOI: https://doi.org/10.3367/UFNe.2022.02.039159

Contents

Abstract. Electromagnetic levitation is a method for containerless high-temperature treatment of metal, semiconductor, and alloy samples. This method is widely used to investigate the thermophysical and thermochemical properties of liquid melts, as well as their crystallization kinetics. An alternating electromagnetic field induces an induction current inside a sample, resulting in a Lorentz force opposing the gravitational force. The Lorentz force lifts the sample, which is heated and melts in a levitation chamber due to the current flowing through it. In this paper, we present an analytical model of the sample levitation process, considering the structure of the electromagnetic levitator coil and options for its optimization for experiments. The kinetics of high-speed solidification of undercooled droplets in the chamber of the electromagnetic levitator is analyzed.

L V Toropova [1, a], **D V Alexandrov** [2, b], **A Kao** [3, c], **M Rettenmayr** [4], **P K Galenko** [4, d]

[1] Laboratory of Mathematical Modeling of Physical and Chemical Processes in Multiphase Media, Institute of Natural Sciences and Mathematics, Ural Federal University, prosp. Lenina 51, 620000 Ekaterinburg, Russian Federation

[2] Laboratory of Multi-Scale Mathematical Modeling, Ural Federal University, prosp. Lenina 51, 620000 Ekaterinburg, Russian Federation

[3] Centre for Numerical Modelling and Process Analysis, University of Greenwich, Old Royal Naval College, Park Row, London, SE10 9LS, UK

[4] Otto-Schott-Institut für Materialforschung, Friedrich-Schiller-Universität Jena, Löbdergraben 32, Jena, 07743, Germany

E-mail: [a] l.v.toropova@urfu.ru, [b] dmitri.alexandrov@urfu.ru, [c] A.Kao@greenwich.ac.uk, [d] peter.galenko@uni-jena.de

Received 25 December 2021, revised 10 February 2022
Uspekhi Fizicheskikh Nauk **193** (7) 770 – 782 (2023)
Translated by V L Derbov

Keywords: electromagnetic levitation, heat-mass transfer, convection, solidification, dendrite, microstructure, levitator

1. Introduction

Since the middle of the 20th century, containerless methods for preparing samples with a predictable structure and properties have been developed and introduced into laboratory practice. Containerless methods for processing liquid melts include spray atomization, drop tubes, melt fluxing, and levitation [1–3]. These methods allow obtaining samples without the external walls of a vessel (crucible, container) to avoid the wall effect on the process of structure formation. The levitation methods of sample processing have become the most widely used.

The basic principle of levitation is to use atmospheric or acoustic pressure or magnetic, electromagnetic, and electrostatic forces acting on an experimental sample (a drop with a diameter of a few millimeters) in order to compensate for the gravity force. Under such compensation, the sample is freely suspended without contact with a liquid or solid medium. In this case, the levitation of macroscopic samples offers a unique possibility of undercooling them and externally controlled stimulation of nucleation.

Achievements in levitation methods became possible mainly due to classical schemes and techniques formulated earlier. One of the deep undercooling methods based on the electromagnetic method of suspending a melt drop has been proposed by Fogel' [4]. The method is based on the relation between the capillary constant and the parameters of the electromagnetic field keeping the sample in a suspended state. This makes it possible to study the behavior of a metal in an electromagnetic field and to determine the acceptable sample size and weight as well as possible temperatures of metals melted using this method. Considering both pioneering and

up-to-date results, we present a review of the main levitation techniques used in experimental setups for obtaining samples with predetermined structure and properties.

2. Methods of levitation

2.1 Acoustic levitation

The operation of an acoustic levitator is based on generating a constant force arising from a high-intensity acoustic field and sufficient to compensate for gravity. When using this approach, the levitation occurs at the positions of acoustic pressure nodes that correspond to the minimum energy.

Such experiments were performed for the first time in the 1930s, when a small sphere levitated under the action of the force that arose due to the acoustic pressure from the standing wave radiation [5]. In this case, according to the nonlinear acoustic theory [6], experimental samples with a mass density greater than that of the surrounding gas must levitate in a high-intensity standing wave of acoustic fields. For position stability, the sample size (from a few submillimeters to a few millimeters) must be much smaller than the sound wavelength (the frequency of the interfering acoustic field varies from 1 to 100 kHz).

For the levitation of metallic systems, i.e., samples with high specific density, the fulfilment of a number of technical requirements is necessary, e.g., an increase in the gas pressure, since the acoustic radiation force linearly grows with pressure [7]. An additional approach to improving the acoustic levitation conditions is to optimize the geometry of the acoustic generator and reflector, since the use of concave surface reflectors can significantly increase the levitation force [8–10].

2.2 Levitation in a DC magnetic field

Levitation in a DC magnetic field implies a stable hovering of a body in spite of gravity. In this case, attraction or repulsion forces arise because of interaction of bodies with magnetic fields. However, according to the Earnshaw theorem [11], there is no stable position for the levitation of a body if the forces acting between the body and the external field are forces of attraction, like those for electrically charged samples in an electric field or for paramagnetic and ferromagnetic materials in a DC magnetic field. The situation changes when considering diamagnetic substances. A diamagnetic sample experiences a repulsive force in a magnetic field, which gives rise to a local minimum of energy in space and, therefore, to a stable position of a suspended drop. This is due to the absence of zero-field magnetization in diamagnetics and the dependence of their state on the magnetic field strength. An advantage of the levitation of diamagnetic materials is the levitation of each individual atom and molecule, since the lifting force is uniformly distributed over the entire sample volume. For melts and liquids, a uniform structure of the sample is typical. In this case, the steady-state levitation reproduces the reduced gravity conditions when there is no convection in the melted sample. This levitation technique allows controlling the levitation force and the sample heating independently, which is a rather complex problem for other types of levitation. Thus, the levitation in static magnetic fields, as a rule, is applied to diamagnetic substances. Nevertheless, experiments with other materials are also known, including water and a number of organic compounds [12–14].

2.3 Electrostatic levitation

The electrostatic levitation (ESL) method is based on Coulomb forces acting on charged particles a few millimeters in diameter under superhigh vacuum conditions (Fig. 1). The experiment is possible with samples that both conduct and do not conduct electric current, placed in an electrostatic field. In this case, various configurations of electrodes are used (e.g., quadrupole or tetrahedral geometry).

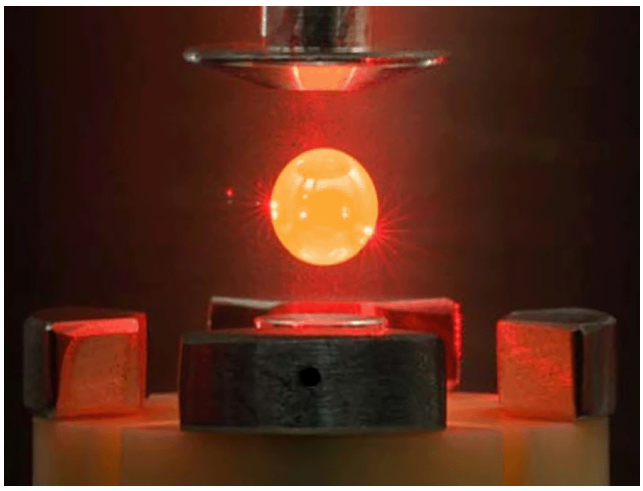

Figure 1. Levitation of a sample in a chamber of an electromagnetic levitator in a superhigh vacuum atmosphere.

The experimental sample is positioned by means of a feedback control system tracing the object location. The feedback control is implemented by either observing the sample optically in combination with computer-aided control of the positioning system or determining the sample position from capacitance measurements and readjusting the voltage applied to the electrodes [15]. During levitation, the sample is heated by a high-power device, consisting of an optical system for focusing laser beams. The sample temperature is measured without contact using pyrometric means [16].

2.4 Electromagnetic levitation

Electromagnetic levitation (EML) is a method of contactless melting and crystallization of metallic, metalloid (with properties intermediate between metals and nonmetals), semiconductor, and alloy samples (of two or more components).

In the containerless method, there is no influence of the walls of the levitation chamber (crucible) on the heterogeneous nucleation of the new phase. After melting, the cyclic processing of the liquid phase in the heating–cooling mode allows purifying the samples of impurities (dust particles, inoculators, cluster formations) that can activate heterogeneous nucleation of crystals. Therefore, with EML, the possibility of uncontrolled heterogeneous nucleation of crystals is maximally eliminated, which allows undercooling samples by a few hundred kelvin [1, 3], thus initiating high-speed crystallization [17].

The principle of EML is based on inducing eddy currents in an electrically conducting sample up to 1 cm in diameter, which is subjected to the action of a time-dependent electromagnetic field (Fig. 2). The method is used to study the properties of melts [18–21], as well as the influence of

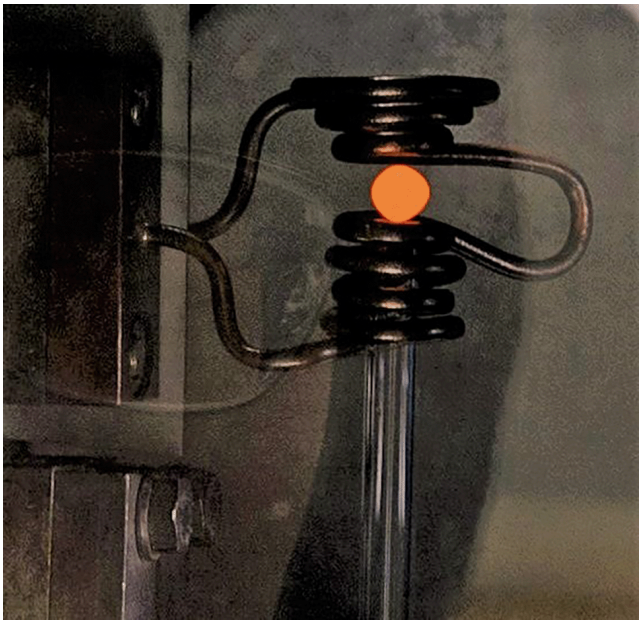

Figure 2. Levitation of a sample in the chamber of an electromagnetic levitator with application of an AC electromagnetic field.

undercooling on the nucleation, growth, and transformation of primary crystals [1, 3].

The distinctive feature of the EML method is the simultaneous presence of two processes: levitation and sample heating. On the one hand, this is an advantage, since no additional source of energy is required for sample melting. On the other hand, the processes of levitation and heating are independently controlled during a very limited time. As a result, EML is widely used in experiments on undercooling macroscopic volumes of melts under the condition that the heterogeneous nucleation caused by the crucible walls be completely eliminated. In this case, surface-initiated nucleation is significantly reduced, because the sample is in a superpure environment. EML is considered in more detail in Section 3.

Concluding the description of the above containerless methods, we note the preference for using the EMS method. This is due to the easy achievement of temperatures above the liquidus, cyclic processing of the liquid phase to deactivate foreign particles or large cluster formations that can serve as centers of spontaneous crystallization, the possibility of dynamic measurements of the thermodynamic and kinetic properties of melts, and the quantitative analysis of the fast crystallization kinetics and phase transformations in the solid state.

2.5 Containerless technique under conditions of reduced gravity and microgravity

The conditions of reduced gravity for conducting experiments with macroscopic metallic samples are created in TEXUS sound rockets or during parabolic flights of European Space Agency airbuses. In both cases, the rocket or airbus begins to dive with its engines turned off from a predetermined height, thereby creating free-fall conditions. Microgravity conditions are present aboard the International Space Station (ISS).

To apply electromagnetic levitation under the conditions of reduced gravity and microgravity, a special facility, TEMPUS (Tiegelfreies Elektro-Magnetisches Prozessieren

Figure 3. Airbus for parabolic flights within the joint programs of the European Space Agency and the German Aerospace Center. On board, there is a scientific laboratory and the TEMPUS facility aimed to measure thermophysical and kinetic properties of liquid metals, as well as crystallization kinetics of metallic, semiconductor, and alloy samples.

Unter Schwerlosigkeit, which in German means Crucible-Free Electromagnetic Processing in the Absence of Gravity Force), has been developed. The facility is installed on an airbus performing parabolic flights (Fig. 3) and in Europe's Columbus module of the ISS. TEMPUS is an instrument for measuring thermodynamic and kinetic properties of melts, such as surface tension, viscosity, and electric conductivity [22–24]. The measurements are carried out both at temperatures above the melting point and in a metastable liquid[1] undercooled below the melting point [22]. These parameters of the material are necessary for quantitative modeling of solidification using the theoretical models presently being developed [17].

A specific feature of using the containerless technique in space is the possibility of using a special medium in which the positioning forces aimed to compensate for perturbing accelerations are approximately three orders of magnitude smaller than the levitation force. As a result, the sample is heated less than when using electromagnetic levitation for the normal gravity force under terrestrial conditions. It is also worth mentioning that, under the conditions of microgravity, the shape of the samples in the course of experiments is close to spherical, which is necessary to measure the mass density of liquid metals with high accuracy. Such experiments become difficult in the gravitational field of Earth, since the levitation forces lead to the deformation of a liquid drop, as well as to dynamic motion of the liquid phase and the appearance of convection in the sample.

Since the transfer processes are strongly affected by Earth's gravitational field, experiments at reduced gravity and microgravity provide high-precision measurements of thermodynamic and kinetic properties of the samples studied in the molten state. In this case, TEMPUS allows studying the kinetics of solidification of undercooled melts. Experiments on undercooling and measuring the velocities of the recales-

[1] A metastable state has higher free energy than that of a stable state. The system can be in a metastable state for an arbitrarily long time without external action and in the absence of internal particles that could nucleate a new, more energy profitable stable state. Such temporal stability of a metastable state exists because of the energy barrier that separates it from the stable state. Long-lived metastable systems include metallic liquids. Thanks to this property, they can be highly undercooled.

cence[2] front motion provide information on the primary crystallization of metastable phases and even on secondary recrystallization into stable phases [25]. The changes in the growth rate as a function of undercooling are important for finding a criterion of microstructure formation, e.g., dendritic and eutectic growth, which are controlled by conductive and convective transfer of heat and mass [26–28]. Let us recall that the term dendrite means a treelike crystalline structure with a main trunk and side branches, growing in the directions of the principal crystallographic axes of the crystal lattice [29, 30]. Dendrite growth, as a rule, is determined by the single-phase mechanism, whereas eutectic growth is determined by nucleation and the joint growth of two or more solid phases.

3. Method of electromagnetic levitation

3.1 Analytical model

EML originates from the induction of eddy currents in a current-conducting material. An experimental sample placed in a levitation coil is subject to the action of a time-dependent magnetic field in accordance with the Lenz rule

$$\nabla \times \mathbf{E} = -\frac{\partial \mathbf{B}}{\partial t}\,, \tag{1}$$

where $\mathbf{E}$ is the electric field strength, $\mathbf{B}$ is the magnetic field induction field, t is the time. The eddy currents produce a magnetic moment $\mathbf{m}$ directed oppositely to the main field, which gives rise to diamagnetic repulsion force $\mathbf{F}_{\mathrm{R}}$ between the sample and the primary field:

$$\mathbf{F}_{\mathrm{R}} = \nabla(\mathbf{mB})\,. \tag{2}$$

If the repulsion force $\mathbf{F}_{\mathrm{R}}$ is equal in magnitude and opposite in direction to the gravity force $\mathbf{F}_G$, then the sample levitates.

Figure 4 schematically shows a levitation coil of conical shape, consisting of five turns from below and two turns from above to stabilize the sample position with the loop radius b_n and height z_n above the reference level. When an alternating current is passed through the coil, the arising electromagnetic field induces eddy currents in the current-conducting system, which gives rise to a repulsive force in the sample and heat release. The levitation process is determined by the Lorentz force $\mathbf{F}_L$ and the absorption of power P, which are defined as

$$\frac{|\mathbf{F}_L|}{|\mathbf{F}_G|} = \frac{3G(x)}{2g\rho\mu_0}\left|(\mathbf{H}\nabla)\mathbf{H}\right|, \tag{3}$$

$$P(x,z) = \frac{3\pi r L(x)}{\sigma_{\mathrm{el}}\mu_0^2}\,\mathbf{H}^2(z)\,, \tag{4}$$

[2] Recalescence is the process of releasing excess latent heat during the transition from a liquid to a solid crystalline state. The region where the transition occurs and the latent heat is released is observed as bright and light, and the region where the transition does not occur yet is seen to be dark. Therefore, the recalescence front is a surface separating the regions of released and still unreleased latent crystallization heat. Usually, the recalescence front coincides with the surface that envelopes the vertices of growing crystals. At a very high undercooling, when the liquid experiences amorphization and transits to a glassy state, the latent heat is frozen in the amorphous phase, which makes it metastable.

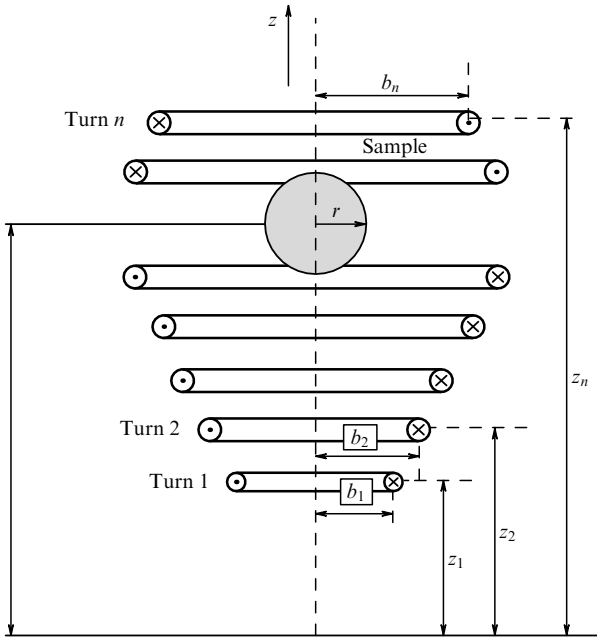

Figure 4. Schematic of a conical levitation coil (r is experimental sample radius, b_n are radii of loops, z_n is height above the reference level).

where the following functions are introduced:

$$G(x) = 1 - \frac{3\sinh(2x) - \sin(2x)}{2x\cosh(2x) - \cos(2x)}\,, \tag{5}$$

$$L(x) = \frac{x\left[\sinh(2x) + \sin(2x)\right]}{\cosh(2x) - \cos(2x)} - 1\,. \tag{6}$$

Here, $\mathbf{H}$ is the magnetic field strength, ρ is the mass density of the sample, μ_0 is the free space permeability, r is the sample radius, σ_{el} is the electrical conduction, g is the free fall acceleration, $x = r\sqrt{\pi\omega\sigma_{\mathrm{el}}g}$, and ω is the magnetic field frequency [31]. Considering the material parameters and applying Eqns (3)–(6), it is possible to calculate the minimum absorption of energy necessary to compensate for the gravity force $\mathbf{F}_G$. The radius of the coil turns is assumed to be much smaller than the sample radius and the loops are assumed to be symmetric.

The force acting on the sample directed oppositely to the gravity force can be expressed as [32, 33]

$$F_L^z(x,z) = 1.5\pi\mu I^2 r^3 G(x) \sum_n \frac{b_n^2}{\left[b_n^2 + (z - z_n)^2\right]^{3/2}} \times \sum_n \frac{b_n^2(z - z_n)}{\left[b_n^2 + (z - z_n)^2\right]^{5/2}}\,, \tag{7}$$

where I is the current strength in the coil. In this case, the power absorption in the sample is expressed as

$$P(x,z) = \frac{3\pi r}{\sigma_{\mathrm{el}}}\,L(x) \sum_n \frac{b_n^2}{\left[b_n^2 + (z - z_n)^2\right]^{3/2}} \times \sum_n \frac{b_n^2(z - z_n)}{\left[b_n^2 + (z - z_n)^2\right]^{5/2}}\,. \tag{8}$$

Figure 5 illustrates the calculated field strength (solid curve) and field gradient (dashed curve) versus the position

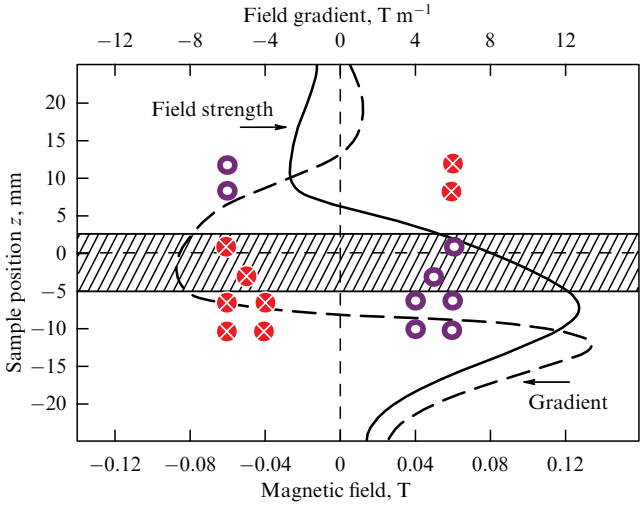

Figure 5. Magnetic field strength (solid curve) and magnetic field gradient (dashed curve) as functions of the sample position (at a current strength of $I = 400$ A in the coil). Sections of the coil turns are shown by color circles allowing for the direction of current. Shadowed area corresponds to the most stable position of the levitating sample. Coil was developed to carry out experiments on gold undercooling [34].

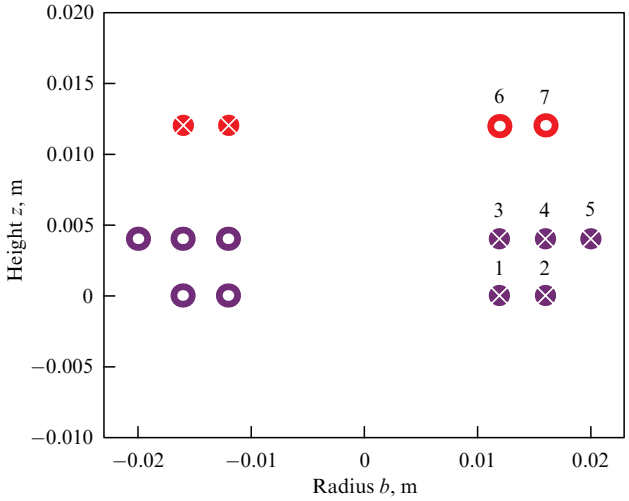

Figure 6. Geometry of the original coil used in the optimization process. Calculation parameters are summarized in the Table.

Table. Parameters of the original coil used after optimizing its geometry.

Loop	Height z_n, m	Radius b_n, m	Turn k_n*
1	0	0.012	1
2	0	0.016	1
3	0.004	0.012	1
4	0.004	0.016	1
5	0.004	0.020	1
6	0.012	0.012	−1
7	0.012	0.016	−1

* Positive/negative values correspond to a conical turn, located above/below the reference level.

of the experimental sample. In this case, the sample moving along the dashed curve can stably levitate.

In equilibrium, the heat transfer to the environment can be assumed to be realized only through radiation; therefore, the sample temperature in the experiment approaches the temperature determined by the heat balance under vacuum conditions as

$$P = Q_{\mathrm{R}}\,, \tag{9}$$

where Q_{R} is the transferred heat given by the Stefan–Boltzmann equation in the form

$$Q_{\mathrm{R}} = 4\pi r^2 \sigma_{\mathrm{SB}} \varepsilon (T^4 - T_0^4)\,. \tag{10}$$

Here, σ_{SB} is the Stefan–Boltzmann constant, ε is the integral emission coefficient of the surface, and T and T_0 are the temperatures of the sample and environment, respectively.

To control the temperature of levitating samples, separate actions of $|\mathbf{F}_L|$ and P are necessary. It follows from Eqns (3)–(6) that the functions $G(x)$ and $L(x)$ have different characteristics relative to the frequency of the AC electromagnetic field, since $|\mathbf{F}_L|$ depends on the product $|(\mathbf{HV})\mathbf{H}|$, and P is proportional to $\mathbf{H}^2$. Therefore, the temperature control is implemented only within a limited time interval (when a suitable frequency of the AC field is chosen) and when the experimental sample moves along the coil symmetry axis z. As is seen from Fig. 4, the turns in the bottom part of the coil are more compressed. Therefore, the magnetic field and the absorption of energy more strongly affect the sample here than in the top part of the coil. However, upon an increase in generator power, the experimental sample lifts up to the region of the greater field gradient and smaller magnetic field strength and, therefore, is cooled. When using coils of different geometries, it is possible to control the sample temperature variation by a few hundred kelvin.

3.2 Electromagnetic levitation coil construction

The processes of sample levitation and heating cannot occur independently of each other. Using various versions of coil configuration allows a wider range of temperature control under the condition of stable sample levitation.

The interrelation between the levitation process and the coil geometry was first studied in Ref. [35], where a metallic sphere in the field created by two identical induction loops was considered. The effect of such parameters as the strength and frequency of the current, sample size, and electric conduction on the optimal coil geometry was also studied [32]. In spite of efforts to formulate a certain coil model for conducting experiments on electromagnetic levitation, the authors of Ref. [35] could not go beyond the conventional 'make and try' practice. For many years, this practice allowed optimizing the coil construction based on the analytical model presented in Section 3.1 and the method of genetic algorithm used to solve the problem of modeling and optimization by a sequential choice, combination, and variation of various desired parameters with the use of mechanisms resembling biological evolution [31].

The construction of the original coil used as the base coil in the optimization process is presented in Fig. 6. This model demonstrated good levitation performance and operation at high temperatures [36, 37]. A sample of Al with a radius of 5 mm in the Ar environment was chosen for the experiment.

With time, a total of 60 generations, each consisting of 40 options, were used to optimize the coil structure [31]. Figure 7 shows the general change in the coil configuration. The change in geometry is seen to occur mainly during the first 10 generations, when the lowest experimental temperature for that time was reached. In addition, the structure of the original coil is 'pancake'-shaped. The final construction

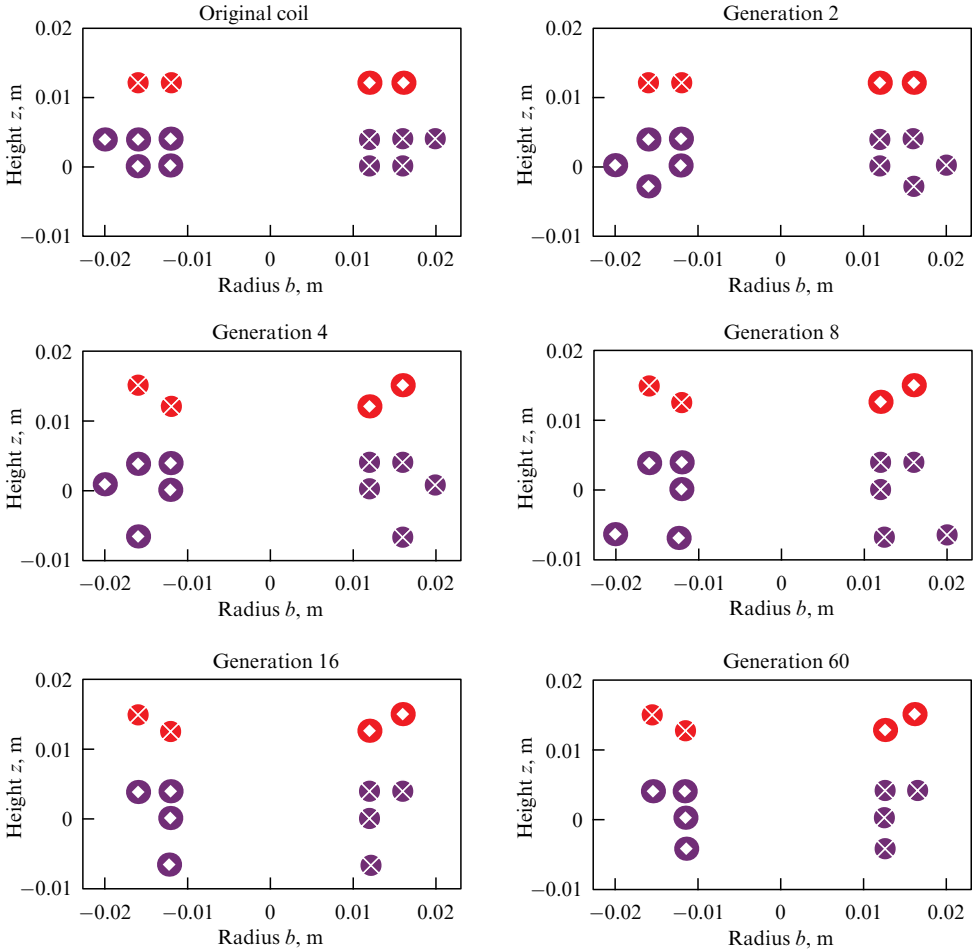

Figure 7. Evolution of the original coil construction over 60 generations. Figure shows examples of the evolution of five generations.

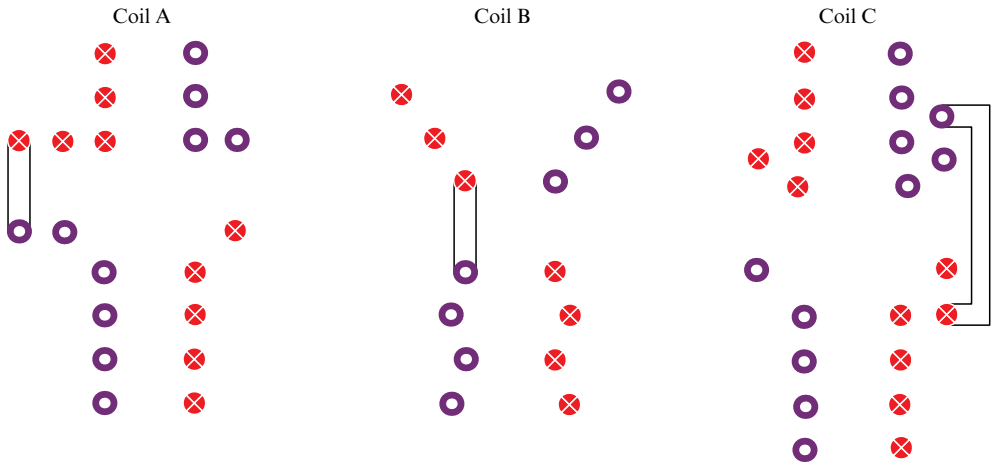

Figure 8. Various geometries of coils used at the Otto Schott Institute of Materials Research, Friedrich Schiller University (Jena, Germany). Lines show configuration changes and the connection of top and bottom parts of the coil.

consists of a smaller number of turns and, generally, has a cylindrical shape more characteristic of a solenoid.

At present, containerless undercooling experiments with metallic samples are being performed in the Otto Schott Institute of Materials Research, Friedrich Schiller University Jena (Germany). Figure 8 schematically shows three geometries of coils made of copper pipes, installed in an EML chamber. The requirements for the coils include the stability of the sample position in the course of its levitation and the maximum attainable temperature of sample heating. Coil B corresponds to the geometry found theoretically by Royer et al. [31]. Coils A and C were developed and passed practical testing at the German Aerospace Center (Cologne).

4. Conduction of experiment

Experiments on heating and cooling pellet samples are carried out in a chamber of an electromagnetic levitator, a general

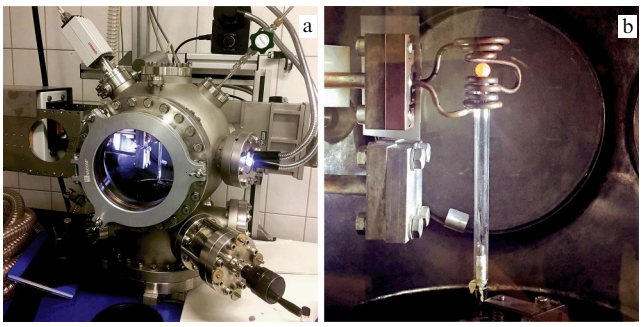

Figure 9. Experimental electromagnetic levitation setup in the Otto Schott Institute of Materials Research, Friedrich Schiller University (Jena, Germany). (a) General view of the EML setup. (b) Sample holder (support) with the cooling system and the alternating current core.

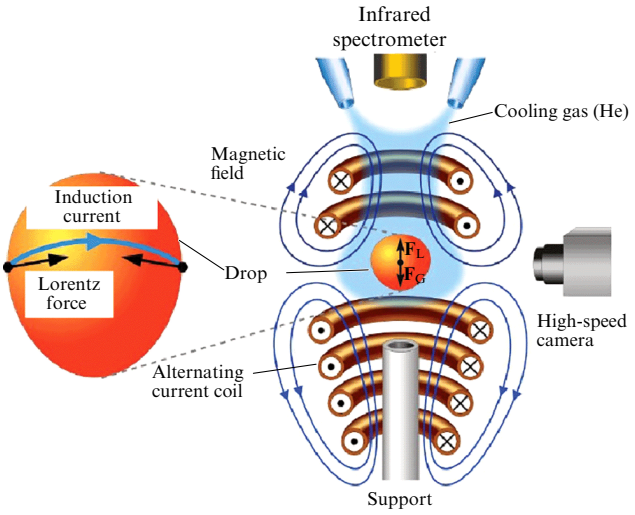

Figure 10. Schematic image of the central part of an electromagnetic levitator chamber for performing containerless experiments. Sample levitates in the core of the EML setup due to the established balance between gravity force $|\mathbf{F}_G|$ and Lorentz force $|\mathbf{F}_L|$, i.e., at $|\mathbf{F}_L| = |\mathbf{F}_G|$. Lorentz force is directed perpendicular to the current.

view of which is shown in Fig. 9a. The crystallization is initiated with a trigger needle made of the same material as the pellet or that occurs due to the spontaneous nucleation of the new phase. In both cases, the initial undercooling is controlled with a pyrometer and the growth rate is then determined from the recalescence front velocity in the sample. In the EML chamber, the sample levitates in a nonuniform electromagnetic field generated by a conical (in some cases, cylindrical) core (Fig. 9b).

The central part of the electromagnetic levitator chamber for containerless experiments is schematically shown in Fig. 10. The levitating sample, with a diameter of up to 1 cm and mass from 300 to 1100 mg, together with the core is placed in a superhigh vacuum chamber, which could be filled with gases, e.g., Ar, He, or $He-H_2$, passed through a liquid nitrogen trap and oxygen-absorbing system.

The core receives energy from a high-frequency generator with a frequency from 300 kHz to 1.2 MHz to provide levitation of samples having different masses. In this case, it is necessary to determine the minimum required power of the generator at which the sample levitates. For this purpose, the generator power is first set to 100 W and turned on for 2 seconds to check the possibility of sample levitation. Since the regulator permits power increments of 10 W, the power is increased stepwise by this value until the minimum power necessary for the sample levitation is found. Then, the temperature is controlled by changing the sample position along the core axis and measured with an infrared pyrometer with an accuracy of 3 K and a reading rate of 100 Hz. Precise measurement of temperature is important to determine the undercooling ΔT. According to the Stefan–Boltzmann radiation law, to put the emitted thermal radiation into correspondence with the current temperature, it is necessary to know the radiating capacity of the experimental sample. In this case, three specific features are taken into account during the measurement. First, the correct radiating capacity depends on the pyrometer or the measured wavelength range, so that the tabulated values can be accepted only when using the pyrometer in the same wavelength range. Second, the radiating capacity changes depending on the degree of oxidation of the sample surface. Third, finally, the radiating capacity changes during a phase transition. In accordance with the above remarks, the pyrometer should be temperature-calibrated in the liquid state, which, however, can yield different values of temperature for the same samples, in spite of the calibration. For this reason, the following formula is used for accurate calculation of the actual temperature based on the equilibrium point according to the Wien displacement law:

$$\frac{1}{T} = \frac{1}{T^{\text{pyro}}} + \frac{1}{T_{\text{L}}} - \frac{1}{T_{\text{L}}^{\text{pyro}}}\,, \tag{11}$$

where T^{pyro} is the temperature, measured with the pyrometer, $T_{\text{L}}^{\text{pyro}}$ is the temperature of the liquidus, measured with the pyrometer, and T_{L} is the temperature of the liquidus corresponding to the phase diagram.

For each cycle, the corrected temperature-time profiles are plotted, from which the undercooling can be calculated. The temperature-time profile in Fig. 11 shows the heating, melting, and crystallization of the sample in the interval between T_{L} (liquidus temperature) and T_{S} (solidus temperature). After heating the melt above T_{L}, the sample is undercooled to the temperature T_{N}, at which the nucleation of crystals is initiated with a trigger needle or spontaneously inside the drop. The crystallization leads to a fast increase in temperature during recalescence. Dendrites, formed at the nucleation point, rapidly grow through the melt volume due to strong undercooling. In the process of heating, the temperature reaches a value between T_{L} and T_{S}, and the interdendritic melt remaining inside the drop solidifies during the 'plateau' under thermodynamic equilibrium conditions. The plateau duration Δt_{pl} is determined by the heat transfer from the sample to the environment (i.e., to the volume of the electromagnetic levitator chamber) and is quantitatively estimated by the temperature-time profile. Time Δt_{pl} is an experimentally controllable parameter, which can vary upon a change in the cooling rate.

5. Solidification of undercooled drops in an electromagnetic levitator

5.1 Structure and velocity of the crystallization front

In the course of experiments, an AC electric current flows through the core and the induced electromagnetic field induces eddy currents in a solid electrically conducting

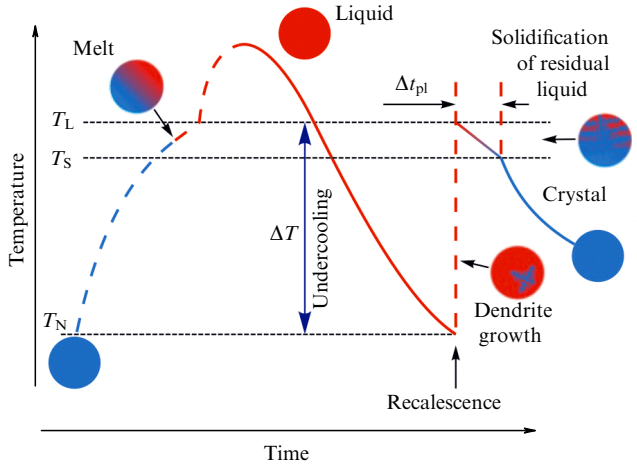

Figure 11. Schematic diagram of temperature variation and formation of the primary structure in drops processed in the EML setup. Variation in temperature in the drop (dashed line from the left): $T < T_S$ — heating, $T_S < T < T_L$ — melting; $T > T_L$ — overheating and deactivation of heterogeneous inclusions. Cooling and crystallization (solid line from the left): $T > T_L$ — cooling of a liquid; $T_N < T < T_L$ — cooling of a metastable liquid; $T = T_N$ — nucleation of crystal(s) at fixed undercooling ΔT and the beginning of propagation of the recalescence front. In the interval $T_N < T \leqslant T_L$ (dashed line from the right), the sample crystallizes during a time of the order of $t \sim 10^{-3} - 10^{-4}$ s, with recording of the recalescence front with a high-speed digital camera. At $T_S \leqslant T \leqslant T_L$ (solid line from the right), the solidification of the residual interdendritic liquid occurs during time Δt_{pl} (subscript 'pl' means plateau). At $T \leqslant T_S$ (solid line from the right), the cooling of the completely solidified sample occurs.

pellet. These currents give rise to the repulsive force (the Lorentz force $\mathbf{F}_L$) directed opposite to the basic field and to heat release, due to which the pellet is melted. When there is a balance between the Lorentz force and gravity force, i.e., $|\mathbf{F}_L| = |\mathbf{F}_G|$, the pellet begins to levitate and simultaneously melts due to the heating. The melted pellet in the form of a liquid drop can then be undercooled to a temperature below the equilibrium solidification temperature due to a cooling gas passed through the working volume of the electromagnetic levitator. Periodic heating and cooling above the liquidus temperature provide the purification of the liquid phase from foreign particles and cluster formations, which can serve as centers of heterogeneous nucleation of crystals.

After the beginning of solidification (initiated by the trigger needle or spontaneous (Fig. 12a)), the released latent heat heats the crystallizing part of the sample with a movable recalescence front (Fig. 12b). This front is a geometric envelope of vertices of primary crystals that usually have a dendritic structure. The heat and mass transfer in the recalescence front control the growth kinetics of such dendritic crystals. The front of high-speed crystallization is recorded using a fast digital camera (see Fig. 10) with a record rate of up to 4×10^5 frames per second. Computer films and images from the fast digital camera allow recording the recalescence front and estimating quantitatively the velocity of its motion in the undercooled drop [1, 38, 39]. A record of the primary crystallization of an undercooled drop in an electromagnetic levitator obtained using the fast camera is shown in Ref. [40].

5.2 Competition and selection of phases

During primary crystallization, a short-lived metastable crystalline phase can arise that transforms into a more stable crystalline phase with heat release, which is observed as secondary recalescence [25]. Thus, during rapid crystallization from a deeply undercooled melt, competition and selection of phases occur. To identify phases in the competition and selection processes during the primary and secondary recalescence, X-ray diffraction analysis was applied directly in the process of sample solidification, as well as during the period of sample cooling in the subsolidus range of temperatures, $T < T_S$ [41, 42]. In particular, the search for disordered phases was carried out, in which the main focus was on the transition from the ordered to disordered phase of an intermetallic compound in the system Ni–Al [43]. The diffraction of synchrotron radiation by levitating samples of the $Ni_{50}Al_{50}$ alloy unambiguously determined the transition from ordered to disordered crystal growth occurring at a critical undercooling of approximately 250 K [44]. The complete transition at critical undercooling was accompanied by a sharp increase in the crystal growth rate of the congruently melting intermetallic phase. This sharp transition in the kinetics of the crystal growth is explained by disorder locking upon nonequilibrium solidification of deeply undercooled melts [45] in correspondence with the theory of kinetic phase transitions [46, 47].

5.3 Amorphization of samples

The affinity to the formation of an amorphous phase and metallic glasses in samples processed in containerless equipment has been under study from the time of the appearance of reliable methods of strong undercooling of macroscopic samples [48, 49]. One of the conditions of metallic glass formation is the short time of freezing the liquid phase with

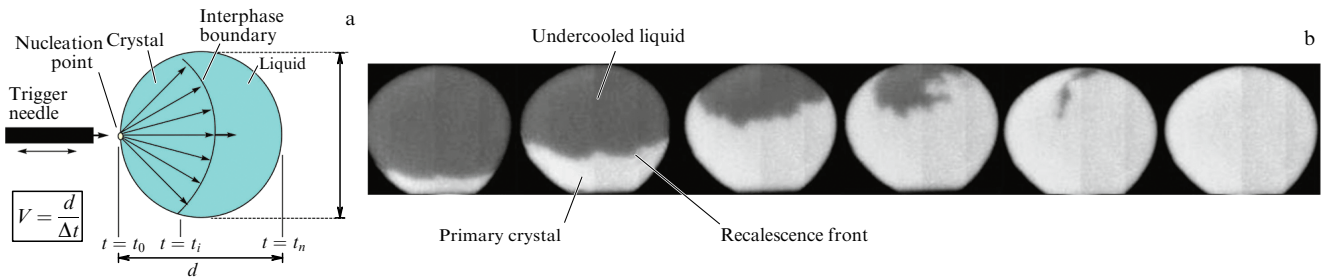

Figure 12. Propagation of the solidification front (interphase boundary, recalescence front) initiated with a trigger needle. (a) Crystal growth velocity V is determined by drop diameter d and time difference Δt, counted from the beginning t_0 to the end t_n of the drop solidification. (b) Time sequence of the solidifying drop in an electromagnetic levitator. Solidification front indicated as interface between solid and liquid phases is an envelope of vertices (dendritic crystals), where the latent heat of crystallization begins to intensely release. This determines the recalescence front, separating the bright (light) region of the crystallizing material and the dark region of undercooled liquid [38].

an anomalous increase in its viscosity compared to the time of waiting for the formation of a crystal nucleus in the liquid volume [50, 51]. A sample in an EML can be greatly undercooled for a long time without spontaneous nucleation of crystals exactly to the high-viscosity liquid state, in which the nucleation of crystals becomes impossible, and the sample becomes amorphous. In this case, the formation of a glass pellet occurs gradually, when the measured rate of crystal growth gradually tends to zero upon a sequential increase in the initial undercooling in the pellet.

Examples of a sharp transition to the amorphous state in samples processed in EML are also well known. For example, samples of $Cu_{50}Zr_{50}$ glasformer were studied under terrestrial conditions and under microgravity [52]. For these conditions, experimental data on the crystallization kinetics were compared with calculations using the model of rapid dendrite growth, considering the results of molecular dynamic modeling of the structure and viscosity changes in the $Cu_{50}Zr_{50}$ melt. Critical undercooling was found, at which the crystallization kinetics is nullified, because the growth of crystals turns out to be impossible, since, due to the structural transition in the melt, individual clusters form long molecular chains, unable to diffuse and attach to the arising solid crystal nuclei [53]. The transition to zero growth kinetics occurs abruptly with the formation of a gel-like state in the entire volume of the sample, which is interpreted as a transition to the amorphous phase, gradually solidifying with a decrease in temperature and the formation of glass samples of the $Cu_{50}Zr_{50}$ system.

Glass samples of typical glasformers (Zr-based vitralloy, Pd-based alloys, and ZrCu-based alloys [54]) are in demand and widely used as highly electrically conductive elements of modern smartphones and tablets, as well as parts of household appliances combining toughness and improved strength properties.

5.4 Liquid phase convection and dendrite growth

When melting a pellet and during its further cyclic processing with EML under terrestrial conditions, an intense convection is induced in the liquid phase of a drop [39, 55–58], which can substantially affect the morphology of the crystals and the kinetics of their growth [39]. The AC magnetic field induces an electric current that causes such a motion of the melt that two spatial tori are formed in the liquid (Fig. 13a). From the bottom side of the drop (near its south pole), the flow in the middle part of the sample is directed downward, and in the top part (near the north pole), it is directed upward. Immediately after the beginning of solidification, the convective flow, having mean velocity U, is directed against the growing dendritic crystals in the bottom part of the drop (Fig. 13b, c). This leads to an increase in the growth rate V and the formation of the most developed main trunks of the dendrites growing against the liquid phase flow, as shown in Fig. 13d. The increase in the rate of the dendrite branches growing against the flow is caused by the intense convective removal of the releasing latent crystallization heat. Calculations of convective structures in the drop processes in EML setups [55, 56, 59] confirm this pattern of convective tori, arising after the melting and during the crystallization of the pellet [38, 60].

To describe the evolution of microstructures in undercooled drops (in particular, to determine the velocity V of the recalescence front and the characteristic size of dendrites R depending on the melt undercooling ΔT), the theory of

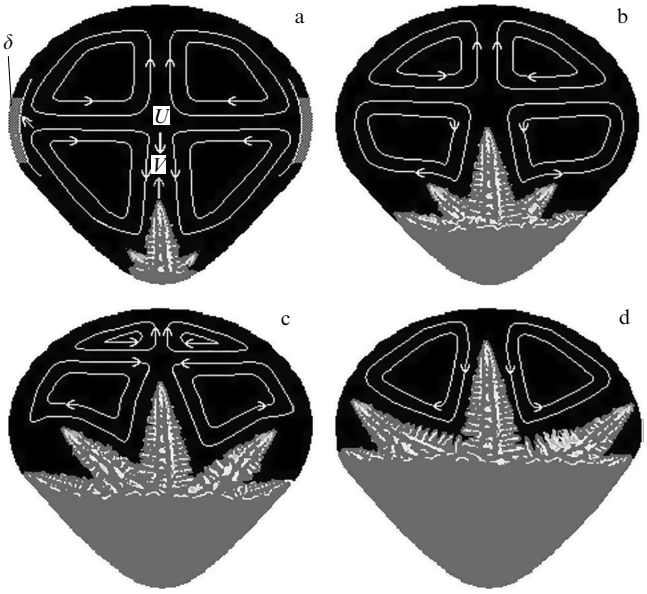

Figure 13. Schematic current lines of liquid phase convection cells during dendrite crystallization of a drop in an electromagnetic levitator [38]. Two-dimensional section of the drop shows the cell structure of the liquid, which is represented by two tori in three spatial dimensions. V is the velocity of the dendrite vertex, U is the averaged velocity of the liquid flow, δ is the thickness of the near-surface layer, in which the maximum current induction and drop heating occur (the so-called skin effect under the action of an alternating electromagnetic field). (a) Direction of the convection flow immediately after the beginning of solidification. (b) Dendrite growth in the incident flow of the bottom convective torus. (c) Gradual degeneration of the top convective torus. (d) Dendrite growth and flow direction at the final stage of sample solidification; the flow direction is still opposite to dendrite growth.

microscopic solubility and the theory of morphological stability are used [61, 62]. To check the theory, a computer simulation is used, e.g., by enthalpy or phase-field methods [63]. The total undercooling $\Delta T = T_M - T_\infty - mC_\infty$ at the dendrite vertex in a binary melt is determined by the contributions

$$\Delta T = \Delta T_T + \Delta T_C + \Delta T_R + \Delta T_K \,, \tag{12}$$

where T_M is the temperature of the phase transformation in a pure liquid, m is the liquidus slope, and C_∞ and T_∞ are the impurity concentration and the temperature in the melt far from the growing dendrite. The thermal $\Delta T_T(V, U, R)$ and the concentration $\Delta T_C(V, U, R)$ undercooling are supplemented with the undercooling $\Delta T_R(R)$ arising at the dendrite vertex because of the curvature of the interphase boundary (the Gibbs–Thomson effect) and the kinetic undercooling $\Delta T_K(V)$ that determines the intensity of atomic kinetics at the dendrite vertex (here, U is the velocity of the liquid flow incident on the dendrite, R is the dendrite vertex diameter). The four above contributions to the total undercooling depend on the spatial geometry of the growth, two-dimensional (2D) or three-dimensional (3D), as well as on the character of the liquid flow (laminar of turbulent) [61, 62, 64, 65]. In the cited papers, analytical expressions for the above contributions to the total undercooling (12) are presented.

The balance of undercooling (12) is the first equation for finding two growth parameters: velocity V and diameter R of the dendrite vertex depending on the driving force ΔT. The second relation is the criterion of stable growth [61, 62,

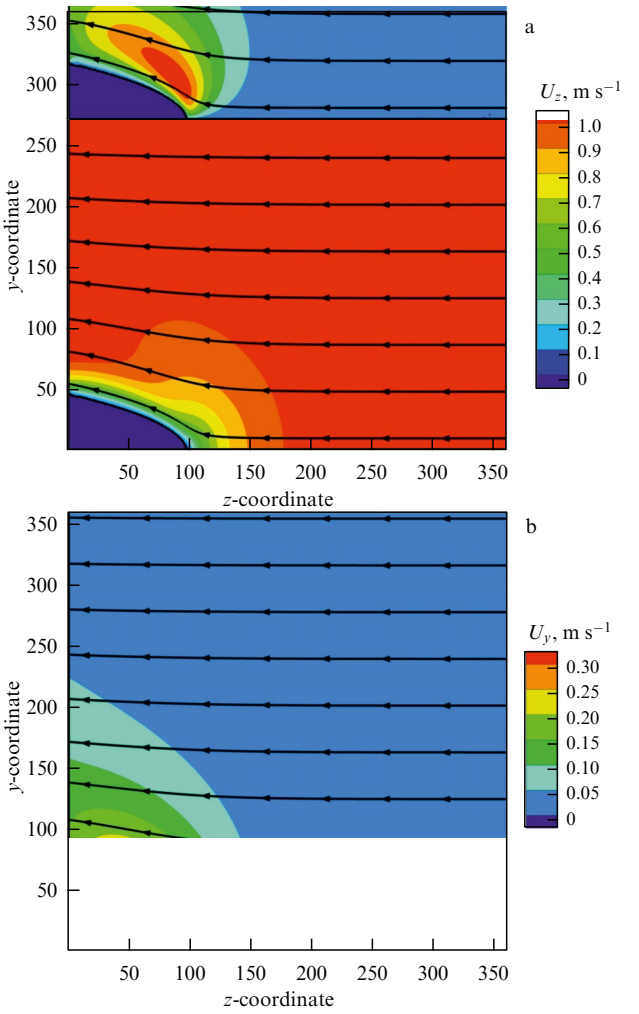

Figure 14. Dendrite vertex growth (bottom-left corner) from an undercooled nickel melt [66]. Liquid flow velocity is 1.08 m s^{-1} at the dendrite vertex at an undercooling of $\Delta T = 106$ K. Coordinates z and y are measured in the number of computational grid nodes. Color scale for velocity components U_z and U_y determines flow velocity in meters per second: (a) z-component of velocity, (b) y-component of velocity.

64, 65]

$$\frac{2d_0 D_T}{R^2 V} = \Lambda(V, U, R)\,, \qquad (13)$$

where d_0 is the capillary constant, and D_T is the thermal diffusivity. Function Λ has different forms for different modes of dendrite crystal growth (slow, moderate, or rapid growth mode, laminar of turbulent liquid flow, 2D or 3D growth geometry). The exact form of the function Λ can be found in Refs [61, 62, 64, 65].

To understand qualitatively the evolution of crystals inside the undercooled drops, we present the results of calculations by the enthalpy method [66]. This method is a computational tool for describing the dynamics of complex-structure interphase boundary motion [67–73].

An example of dendritic growth in an established laminar melt flow is shown in Fig. 14, depicting the morphology of a dendrite vertex and the components of the flow velocity (in projection on the coordinate axes y and z). Since the dendrite is a solid crystalline phase, the liquid flows around it, with a stagnation point at the very vertex and higher velocities inside

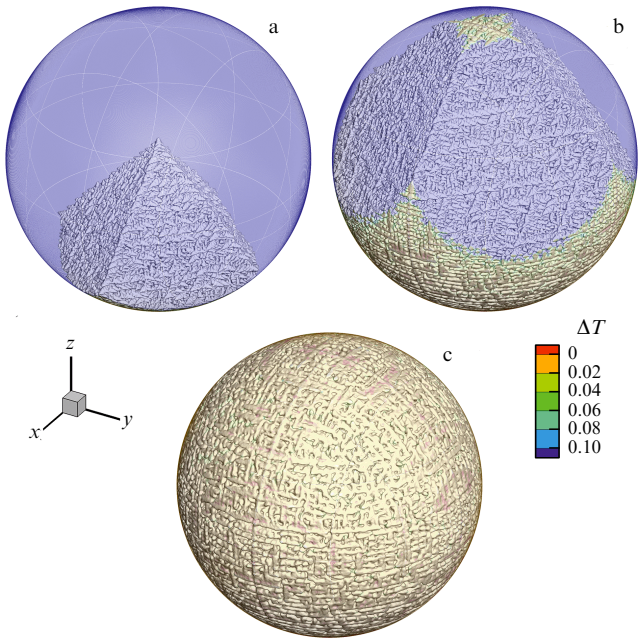

Figure 15. Dendrite growth from a pure melt of undercooled nickel [74, 75] at different stages of solidification: (a) early recalescence, (b) late recalescence, (c) stage of enlargement of primary dendrites. Color scale shows the undercooling ΔT in units L/c_p, where L is the latent crystallization heat [J m^{-3}], c_p is the heat capacity at constant pressure [J (m^3 K)$^{-1}$].

the thermal boundary layer. However, since the relative velocity at the interface is zero, a viscous boundary layer is formed between the surface and the region of higher velocities.

Figure 15 illustrates the microstructure evolution during the solidification of an undercooled drop of pure nickel obtained by computer simulation [74] using the enthalpy method. The visualization of this process in time is presented in Ref. [75]. The simulation results were verified by comparing them with experimental observations [76, 77] on measuring the surface temperature of a solidifying drop. Note that, the greater the undercooling, the smaller the characteristic distance between the dendrites and, therefore, the greater the curvature of their vertices. This regularity makes it possible to affect the microstructure of a solidifying sample by varying the undercooling.

6. Conclusion

The levitation technique allows sample processing in a suspended state, which eliminates the effect of external walls of the crucible or container on the processing (heating–melting–cooling–crystallization–further cooling). Such a technique is by definition containerless [3, 57]. By using it, foreign particles, inoculators, and centers of a new phase nucleation become deactivated after a few cycles of sample heating and cooling. The probability of heterogeneous nucleation is substantially reduced, and the sample can be undercooled relative to the equilibrium temperature of crystallization/melting or solid-phase transformation by many tens or hundreds of kelvin [1]. The driving force of the phase transformation arising in this case turns out to be so strong that it leads to a fast motion of the crystallization front or phase transformation in the solid state [17].

The paper gives a brief review of acoustic and electrostatic levitation methods and the levitation of samples in a DC magnetic field. Special attention is paid to the method of electromagnetic levitation used to study the properties of liquid metals and melts and the kinetics of their crystallization, as well as to obtain samples with a predetermined structure and properties. Specific features of levitation of samples and their processing are considered under terrestrial conditions, as well as under the conditions of reduced gravity during parabolic flights of airbuses of the European Space Agency and under microgravity available aboard the International Space Station.

The conditions of sample crystallization in electromagnetic levitators were specially considered, which demonstrate the dominant role of transfer processes in the microstructure formation of the materials under study. Recording the recalescence front (as the envelope of vertices of the growing dendritic crystals) with a high-speed digital camera and controlling the beginning and the end of crystallization pyrometrically provide unique information for checking and improving theoretical models of primary crystallization and the formation of secondary structures in metallic and alloy samples.

The present paper briefly presents the methods of containerless processing of samples, especially the method of electromagnetic levitation with the processed structure of samples in the melted, crystallizing, and post-recalescence period. An excellent addition to the review given here is the article by D M Herlach [78], which provides an extensive historical and technical excursus to the field of sample processing by containerless methods. In particular, when describing the processing of drops in EML, the review by D M Herlach offers a wider view of some phenomena occurring in the process of drop structure formation. For example, a detailed description is given for the effect of the granular structure refinement observed in the range of very small undercooling values or at the maximum values of undercooling reached before the beginning of drop crystallization.

While working on the manuscript of this article, we received bitter news about the sudden death of one of the main experts in the field of levitation and quantitative measurements of high-speed solidification, Dieter Matthias Herlach (German Aerospace Center, Cologne). Professor Herlach created a school of numerous specialists in high-speed solidification. This school consists of about 30 specialists, including experimenters, theorists, and numerical modelers, who are currently working all over the world, from Germany, Great Britain, and France to China, India, Peru, and Russia. Professor Herlach's school effectively develops and interacts in the framework of joint projects, systematic meetings, seminars, and specialized sections of conferences. We dedicate this article about levitators to the blessed memory of Dieter Matthias Herlach, whose activity, efficiency, and concentration on achieving results have always aroused our admiration.

This paper was supported by the Russian Science Foundation (grant no. 21-79-10012).

References

1. Herlach D, Galenko P, Holland-Moritz D *Metastable Solids from Undercooled Melts* (Amsterdam: Elsevier, 2007); Translated into Russian: *Metastabil'nye Materialy iz Pereokhlazhdennykh Rasplavov* (Moscow–Izhevsk: RKhD, Inst. Komp. Issled., 2010)
2. Lavernia E J, Srivatsan T S *J. Mater. Sci.* **45** 287 (2010)
3. Herlach D M, Matson D M (Eds) *Solidification of Containerless Undercooled Melts* (Weinheim: Wiley-VCH, 2010)
4. Fogel A A *Induktsionnyi Metod Uderzhaniya Zhidkikh Metallov vo Vzveshennom Sostoyanii* (Induction Method for Holding Liquid Metals in Suspension) (Books Collection of High-Frequency Thermist, Issue 14) 4th ed., revised and enlarg. (Leningrad: Mashinostroenie, 1979)
5. King L V *Proc. R. Soc. Lond. A* **147** 212 (1934)
6. Landau L D, Lifshitz E M *Fluid Mechanics* (Oxford: Pergamon Press, 1987); Translated from Russian: *Gidrodinamika* (Moscow: Nauka, 1988)
7. Trinh E H *Rev. Sci. Instrum.* **56** 2059 (1985)
8. Ohsaka K, Trinh E H, Glicksman M E *J. Cryst. Growth* **106** 191 (1990)
9. Ansell S et al. *Phys. Rev. Lett.* **78** 464 (1997)
10. Xie W-J, Wei B-B *Chinese Phys. Lett.* **18** 68 (2001)
11. Jackson J D *Classical Electrodynamics* 2nd ed. (New York: Wiley, 1975)
12. Berry M V, Geim A K *Eur. J. Phys.* **18** 307 (1997)
13. Beaugnon E, Tournier R *Nature* **349** 470 (1991)
14. Weilert M A et al. *Phys. Rev. Lett.* **77** 4840 (1996)
15. Rulison A J, Rhim W-K *Rev. Sci. Instrum.* **65** 695 (1994)
16. Felici N-J *Rev. Gen. de l'Electricite* **75** 1145 (1966)
17. Galenko P K, Jou D *Phys. Rep.* **818** 1 (2019)
18. Amaya G E, Patchett J A, Abbaschian G J, in *Grain Refinement in Castings and Welds: Proc. of a Symp., St. Louis, Missouri, October 25–26, 1982* (Eds G J Abbaschian, S A David) (Warrendale, PA: Metallurgical Soc. AIME, 1983)
19. Schade J, McLean A, Miller W A, in *Undercooled Alloy Phases: Proc. of the 1986 Hume-Rothery Memorial Symp.* (Warrendale, PA: Metallurgical Soc. AIME, 1987)
20. Arpaci E, Ph.D. Thesis (Berlin: Freie Univ. Berlin, 1984)
21. Keene B J et al. *Metall. Trans. B* **17** 159 (1986)
22. Brillo J *Thermophysical Properties of Multicomponent Liquid Alloys* (Berlin: De Gruyter, 2016)
23. Egry I et al. *Adv. Eng. Mater.* **5** 819 (2003)
24. Mohr M et al. *Microgravity Sci. Technol.* **31** 177 (2019)
25. Hartmann H et al. *J. Appl. Phys.* **103** 073509 (2008)
26. Alexandrov D V, Galenko P K, Toropova L V *Philos. Trans. R. Soc. A* **376** 20170215 (2018)
27. Toropova L V et al. *J. Cryst. Growth* **535** 125540 (2020)
28. Alexandrov D V et al. *Russ. Metall.* **2019** 787 (2019)
29. Chernov A A *Modern Crystallography* (Berlin: Springer-Verlag, 1984); Translated from Russian: *Sovremennaya Kristallografiya* Vol. 3 (Moscow: Nauka, 1980)
30. Fedorov O P *Protsessy Rosta Kristallov: Kinetika, Formoobrazovanie, Neodnorodnosti* (Crystal Growth Processes: Kinetics, Shaping, Inhomogeneities) (Kyiv: Naukova Dumka, 2010)
31. Royer Z L et al. *J. Appl. Phys.* **113** 214901 (2013)
32. Fromm E, Jehn H *Br. J. Appl. Phys.* **16** 653 (1965)
33. Fromm E, Jehn H *Z. Met.* **58** 566 (1967)
34. Sauerland S, Ph.D. Thesis (Aachen, Germany: RWTH Aachen, 1993)
35. Okress E C et al. *J. Appl. Phys.* **23** 545 (1952)
36. Moghimi Z A, Halali M, Nusheh M *Metall. Mater. Trans. B* **37** 997 (2006)
37. Kermanpur A, Jafari M, Vaghayenegar M *J. Mater. Process. Technol.* **211** 222 (2011)
38. Funke O et al. *J. Cryst. Growth* **297** 211 (2006)
39. Binder S, Galenko P K, Herlach D M *Philos. Mag. Lett.* **93** 608 (2013)
40. Reinartz M, Galenko P K, https://archive.org/details/droplet-processed-in-eml
41. Shuleshova O et al. *Europhys. Lett.* **86** 36002 (2009)
42. Shuleshova O et al. *Int. J. Cast Met. Res.* **22** 286 (2013)
43. Greer A L, Assadi H *Mater. Sci. Eng. A* **226–228** 133 (1997)
44. Hartmann H et al. *Europhys. Lett.* **87** 40007-1-4 (2009)
45. Boettinger W J, Aziz M J *Acta Metall.* **37** 3379 (1989)
46. Chernov A A *Sov. Phys. JETP* **26** 1182 (1968); *Zh. Eksp. Teor. Fiz.* **53** 2090 (1967)

47. Galenko P K et al. *Philos. Trans. R. Soc. A* **376** 20170207 (2018)
48. Kui H W, Greer A L, Turnbull D *Appl. Phys. Lett.* **45** 615 (1984)
49. Gillessen F, Herlach D M *Mater. Sci. Eng.* **97** 147 (1988)
50. Turnbull D *J. Appl. Phys.* **21** 1022 (1950)
51. Turnbull D *Contemp. Phys.* **10** 473 (1969)
52. Galenko P K et al. *Philos. Trans. R. Soc. A* **377** 20180205 (2019)
53. Galenko P K et al. *J. Cryst. Growth* **532** 125411 (2020)
54. Kharanzhevskiy E V et al. *Philos. Trans. R. Soc. A* **380** 20200321 (2022)
55. Flemings M C et al. "Levitation observation of dendrite evolution in steel ternary alloy rapid solidification (LODESTARS)" NASA Science Requirement Document LODESTARS-RQMT-0001 (Washington, DC: NASA, 2003)
56. Matson D M, Hyers R W, Volkmann Th *J. Jpn. Soc. Microgravity Appl.* **27** (4) 238 (2010)
57. Hyers R W, in *Solidification of Containerless Undercooled Melts* (Eds D M Herlach, D M Matson) (Weinheim: Wiley-VCH, 2012) p. 31
58. Meister T et al. *Control Eng. Pract.* **11** (2) 117 (2003)
59. Bojarevich V, Kao A, Pericleous K *Solidification of Containerless Undercooled Melts* (Eds D M Herlach, D M Matson) (Weinheim: Wiley-VCH, 2012) p. 321
60. Galenko P K et al. *Mater. Sci. Eng. A* **375–377** 488 (2004)
61. Alexandrov D V, Galenko P K *Phys. Usp.* **57** 771 (2014); *Usp. Fiz. Nauk* **184** 833 (2014)
62. Alexandrov D V, Galenko P K *Philos. Trans. R. Soc. A* **379** 20200325 (2021)
63. Subhedar A, Galenko P K, Varnik F *Philos. Trans. R. Soc. A* **378** 20190540 (2020)
64. Toropova L V, Alexandrov D V, Galenko P K *Math. Meth. Appl. Sci.* **44** 12139 (2021)
65. Alexandrov D V et al. *J. Phys. Condens. Matter* **33** 443002 (2021)
66. Kao A et al. *JOM* **72** 3123 (2020)
67. Tong X et al. *Phys. Rev. E* **63** 061601 (2001)
68. Galenko P K et al., in *Solidification and Crystallization* (Ed. D M Herlach) (Weinheim: Wiley-VCH, 2004)
69. Ramirez J C, Beckermann C *Acta Mater.* **53** 1721 (2005)
70. Jeong J-H, Goldenfeld N, Dantzig J A *Phys. Rev. E* **64** 041602 (2001)
71. Galenko P K et al., in *Computational Modeling and Simulation of Materials III. Proc. of the 3rd Intern. Conf., Acireale, Sicily, Italy, May 30–June 4, 2004* Pt. B (Eds P Vincenzini, A Lami, F Zerbetto) (Faenza: Techna Group, 2004) p. 565
72. Galenko P K et al. *Acta Mater.* **55** 6834 (2007)
73. Galenko P K et al. *Acta Mater.* **57** 6166 (2009)
74. Gao J et al. *J. Cryst. Growth* **471** 66 (2017)
75. Kao A, https://archive.org/details/droplet-enthalpy-method
76. Gao J et al., in *Solidification of Containerless Undercooled Melts* (Eds D M Herlach, D M Matson) (Weinheim: Wiley-VCH, 2012)
77. Gao J et al. *Acta Mater.* **103** 184 (2016)
78. Herlach D M, in *Solidification of Containerless Undercooled Melts* (Eds D M Herlach, D M Matson) (Weinheim: Wiley-VCH, 2012)